Supporting Information

Exploration of Photocatalytic Overall Water Splitting Mechanisms in the Z-scheme SnS_2/*β*-As Heterostructure

Xuefeng Chen,[a,b] Wenna Han,[a,b] Zhizhong Tian,[a,b] Qian Yue,[a,b] Chengxiao Peng,*[a,b] Chao Wang,*[a,b] Bing Wang,[a,b] Huabing Yin,[a,b] and Qinfen Gu*[c]

[a.] *Institute for Computational Materials Science, School of Physics and Electronics, Henan University, Kaifeng, 475004, China.*

[b.] *International Joint Research Laboratory of New Energy Materials and Devices of Henan Province, Kaifeng, 475004, China.*

[c.] *Australian synchrotron, ANSTO, 800 Blackburn Rd, Clayton, 3168, VIC, Australia.*

Chengxiao Peng - Email: pengcx@vip.henu.edu.cn

Chao Wang - Email: Wangchao@vip.henu.edu.cn

Qinfen Gu - Email: Qinfeng@ansto.gov.au

Gibbs free energy change of HER and OER

The Gibbs free energy change ΔG of HER and OER can be calculated by the formula proposed by Nørskovet[1]:

$$\Delta G = \Delta E + \Delta E_{ZPE} - T\Delta S + \Delta G_U + \Delta G_{PH} \quad (1)$$

where ΔE is the reaction energy calculated by the DFT. ΔE_{ZPE} is the zero-point energy by harmonic vibrational frequency calculations. ΔS is the entropy difference between the adsorbed state and the gas phase. T is the system temperature (298.15 K). $\Delta G_U = -eU$, U is the external potential relative to the standard hydrogen electrode. ΔG_{pH}($\Delta G_{pH} = K_B T \times \ln 10 \times \text{pH}$) represents the free energy contributed in different pH concentrations.

The equations involved in HER can be expressed as[2-3]:

$$* + H^+ + e^- \rightarrow H^* \tag{2}$$

$$H^* + H^+ + e^- \rightarrow * + H_2 \tag{3}$$

$$\Delta G_h = G(H^*) - G(*) - 0.5G(H_2) + 0.059 \times pH - eU \tag{4}$$

$$\Delta G'_h = G(*) - G(H^*) + 0.5G(H_2) + 0.059 \times pH - eU \tag{5}$$

The equations involved in OER can be expressed as:

OER-I[2-3]:

$$* + H_2O \rightarrow OH^* + H^+ + e^- \tag{6}$$

$$OH^* \rightarrow O^* + H^+ + e^- \tag{7}$$

$$O^* + H_2O \rightarrow OOH^* + H^+ + e^- \tag{8}$$

$$OOH^* \rightarrow * + O_2 + H^+ + e^- \tag{9}$$

$$\Delta G_1 = G(OH^*) + 0.5G(H_2) - G(*) - G(H_2O) - 0.059 \times pH - eU \tag{10}$$

$$\Delta G_2 = G(O^*) + 0.5G(H_2) - G(OH^*) - 0.059 \times pH - eU \tag{11}$$

$$\Delta G_3 = G(OOH^*) + 0.5G(H_2) - G(O^*) - G(H_2O) - 0.059 \times pH - eU \tag{12}$$

$$\Delta G_4 = G(*) + G(O_2) + 0.5G(H_2) - G(OOH^*) - 0.059 \times pH - eU \tag{13}$$

OER-II[4-8]:

$$* + H_2O \rightarrow OH^* + H^+ + e^- \tag{14}$$

$$OH^* \rightarrow O^* + H^+ + e^- \tag{15}$$

$$O^* + H_2O \rightarrow O^*OH^* + H^+ + e^- \tag{16}$$

$$O^*OH^* \rightarrow O^*O^* + H^+ + e^- \tag{17}$$

$$O^*O^* \rightarrow OO^* \tag{18}$$

$$OO^* \rightarrow * + O_2 \tag{19}$$

$$\Delta G_1 = G(OH^*) + 0.5G(H_2) - G(*) - G(H_2O) - 0.059 \times pH - eU \tag{20}$$

$$\Delta G_2 = G(O^*) + 0.5G(H_2) - G(OH^*) - 0.059 \times pH - eU \tag{21}$$

$$\Delta G_3 = G(O^*OH^*) + 0.5G(H_2) - G(O^*) - G(H_2O) - 0.059 \times pH - eU \tag{22}$$

$$\Delta G_4 = G(O^*O^*) + 0.5G(H_2) - G(O^*OH^*) - 0.059 \times pH - eU \tag{23}$$

$$\Delta G_5 = G(OO^*) - G(O^*O^*) \tag{24}$$

$$\Delta G_6 = G(*) + G(O_2) - G(OO^*) \tag{25}$$

OER-III[6-7, 9]:

$$* + H_2O \rightarrow OH^* + H^+ + e^- \tag{26}$$

$$OH^* + H_2O \rightarrow HOOH^* + H^+ + e^- \tag{27}$$

$$HOOH^* \rightarrow OOH^* + H^+ + e^- \tag{28}$$

$$OOH^* \rightarrow * + O_2 + H^+ + e^- \tag{29}$$

$$\Delta G_1 = G(OH^*) + 0.5G(H_2) - G(*) - G(H_2O) - 0.059 \times pH - eU \tag{30}$$

$$\Delta G_2 = G(HOOH^*) + 0.5G(H_2) - G(OH^*) - G(H_2O) - 0.059 \times pH - eU \tag{31}$$

$$\Delta G_3 = G(OOH^*) + 0.5G(H_2) - G(HOOH^*) - 0.059 \times pH - eU \tag{32}$$

$$\Delta G_4 = G(*) + G(O_2) + 0.5G(H_2) - G(OOH^*) - 0.059 \times pH - eU \tag{33}$$

where * represents the active adsorption sites on the SnS_2/β-As heterostructure, and H^*, OH^*, O^*, OOH^*, O^*OH^*, O^*O^*, OO^*, $HOOH^*$ represent the adsorption states during the redox process, respectively.

The solar-to-hydrogen (STH) efficiency

The solar-to-hydrogen (STH) efficiency is evaluated in the entire solar spectrum. The efficiency of light absorption is defined as[10]:

$$\eta_{abs} = \frac{\int_{E_g}^{\infty} p(h\omega)d(h\omega)}{\int_0^{\infty} p(h\omega)d(h\omega)} \tag{34}$$

where E_g is the bandgap of materials and $p(h\omega)$ is the AM1.5G solar energy flux at the photon energy $h\omega$. The efficiency of carrier utilization is defined as:

$$\eta_{cu} = \frac{\Delta G \int_{E}^{\infty} \frac{p(h\omega)}{h\omega} d(h\omega)}{\int_{E_g}^{\infty} p(h\omega) d(h\omega)} \tag{35}$$

$$E = \begin{cases} E_g, (\chi(H_2) \geq 0.2, \chi(O_2) \geq 0.6) \\ E_g + 0.2 - \chi(H_2), (\chi(H_2) < 0.2, \chi(O_2) \geq 0.6) \\ E_g + 0.6 - \chi(O_2), (\chi(H_2) \geq 0.2, \chi(O_2) < 0.6) \\ E_g + 0.8 - \chi(H_2) - \chi(O_2), (\chi(H_2) < 0.2, \chi(O_2) < 0.6) \end{cases} \tag{36}$$

here ΔG is the water decomposition potential difference of 1.23 eV, and E is the photon energy that can actually be used for water splitting. The potential difference between the CBM-(β-As) and redox potential of H^+/H_2 ($\chi(H_2)$) is 0.81 eV, while the potential difference between the VBM-(SnS_2) and redox potential of H_2O/O_2 ($\chi(O_2)$) is 1.77 eV at pH = 0, respectively[11].

Therefore, the STH efficiency is defined as:

$$\eta_{STH} = \eta_{abs} \times \eta_{cu} \tag{37}$$

Spectral absorption

The interaction between photons and electrons in semiconductors can be understood as time-varying perturbations of ground-state electrons[12]. Interband excited state transitions can induce common spectra of occupied and unoccupied states, and their optical properties are mainly determined by dielectric function ε[13]. The imaginary part ε_2 can be estimated by the momentum matrix element between the occupied and unoccupied wave functions, while the real part ε_1 can be obtained from ε_2 by Kramers-Kronig transformation[14].

$$\varepsilon_2 = \frac{2e^2\pi}{\Omega\varepsilon_0}\sum_{k,v,c}|\langle\psi_k^c|\boldsymbol{u}\bullet\boldsymbol{r}|\psi_k^v\rangle|^2\,\delta(E_k^c - E_k^v - E) \quad (38)$$

$$\varepsilon_1 = 1 + \frac{2}{\pi}\,p\int_0^{\infty}\frac{\omega'\varepsilon_2(\omega')}{\omega'^2-\omega^2}d\omega' \quad (39)$$

where Ω, ω, v, and c are the unit-cell volume, photon frequency, valence bands, and conduction bands, respectively. $\boldsymbol{u}$ and $\boldsymbol{r}$ respectively represent the polarization vector of the incident electric field and the radius of the electron vector. The optical absorption coefficient $\alpha(\omega)$ of SnS_2, β-As, and SnS_2/β-As heterostructure can then be calculated from ε_1 and ε_2[15].

$$\alpha(\omega) = \sqrt{2}\omega\left[\sqrt{\varepsilon_1(\omega)^2+\varepsilon_2(\omega)^2} - \varepsilon_1(\omega)\right]^{1/2} \quad (40)$$

Three SnS_2/β-As heterostructure configurations

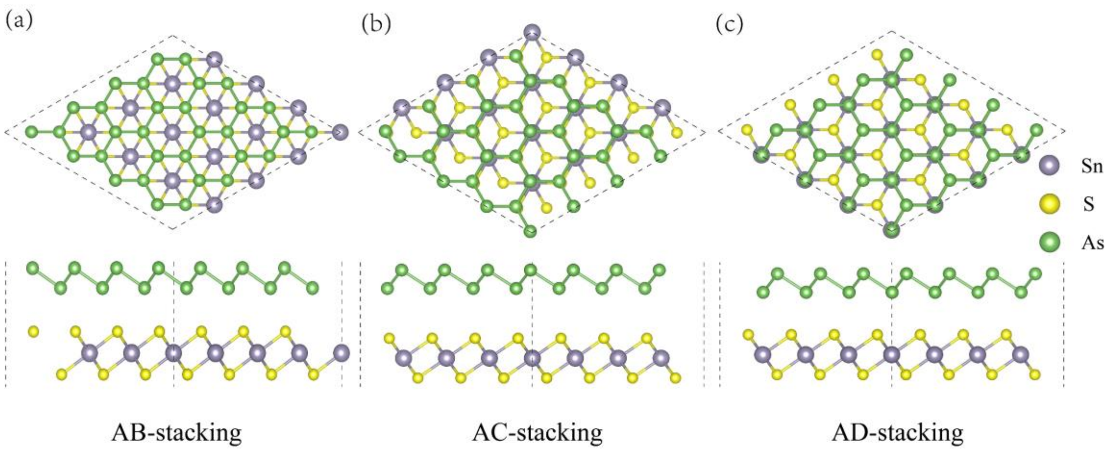

Figure S1 Top (upper panel) and side (lower panel) views of SnS_2/β-As heterostructures with (a) AB-stacking, (b) AC-stacking and (c) AD-stacking.

Work function

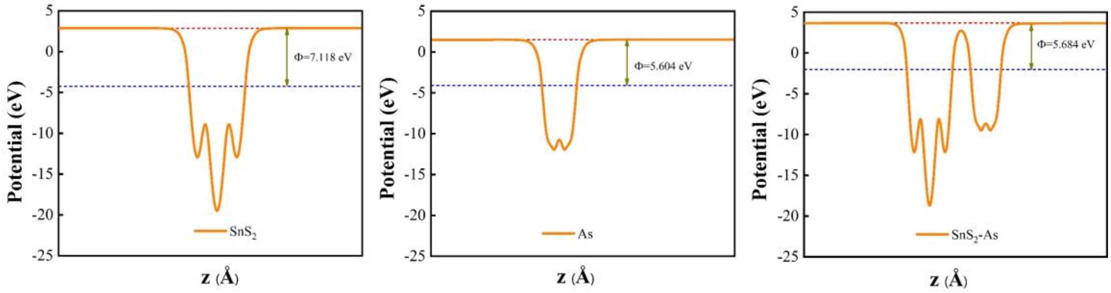

Figure S2 Work functions of SnS_2, *β*-As and SnS_2/*β*-As nanosheets using the HSE06 hybrid functional method; the red and blue lines represent the vacuum and Fermi levels, respectively.

Water adsorption

By adsorbing a water molecule at different sites, the following four adsorption configurations are obtained after optimization. It can be seen that there is only one adsorption site for the water molecule on the surface of the *β*-As layer with an adsorption energy of -0.189 eV (Figure S3a). While there are two adsorption sites in the SnS_2 layer, namely the top of the S atom and Sn atom (Figure S3c,d) in the six-membered ring with adsorption energy of -0.164 and -0.162 eV, respectively. In addition, the water molecule has an adsorption energy of 0.685 eV between the *β*-As layer and the SnS_2 layer (Figure S3b). Because the adsorption energy on both layers is negative and the adsorption energy between layers is positive, it means that water molecules can be stably adsorbed on the surface of the SnS_2/*β*-As heterostructure and participate in the decomposition reaction of water but cannot occur between layers.

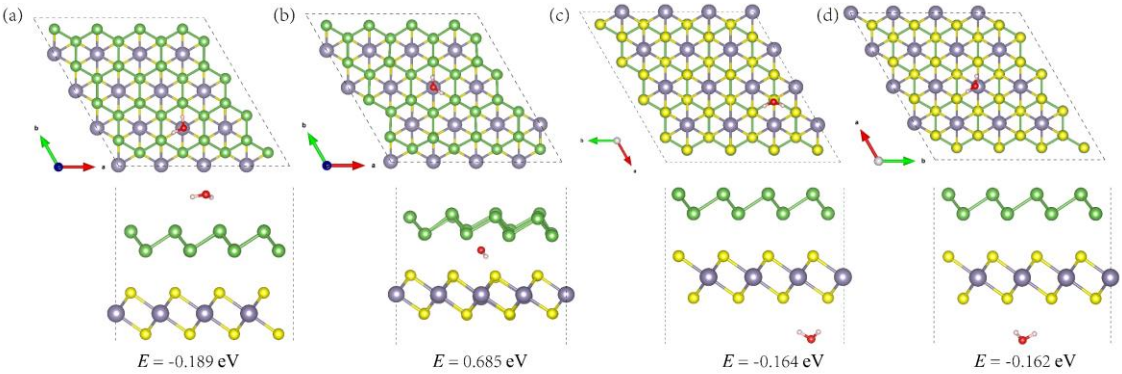

Figure S3 Adsorption of water molecules at different sites in the SnS_2/β-As heterostructure, (a) six-membered ring center on the surface of the β-As layer, (b) between the β-As layer and the SnS_2 layer, (c) above the S atom in the six-membered ring center on the surface of the SnS_2 layer, and (d) above the Sn atom in the six-membered ring center on the surface of the SnS_2 layer.

HER and OER mechanisms

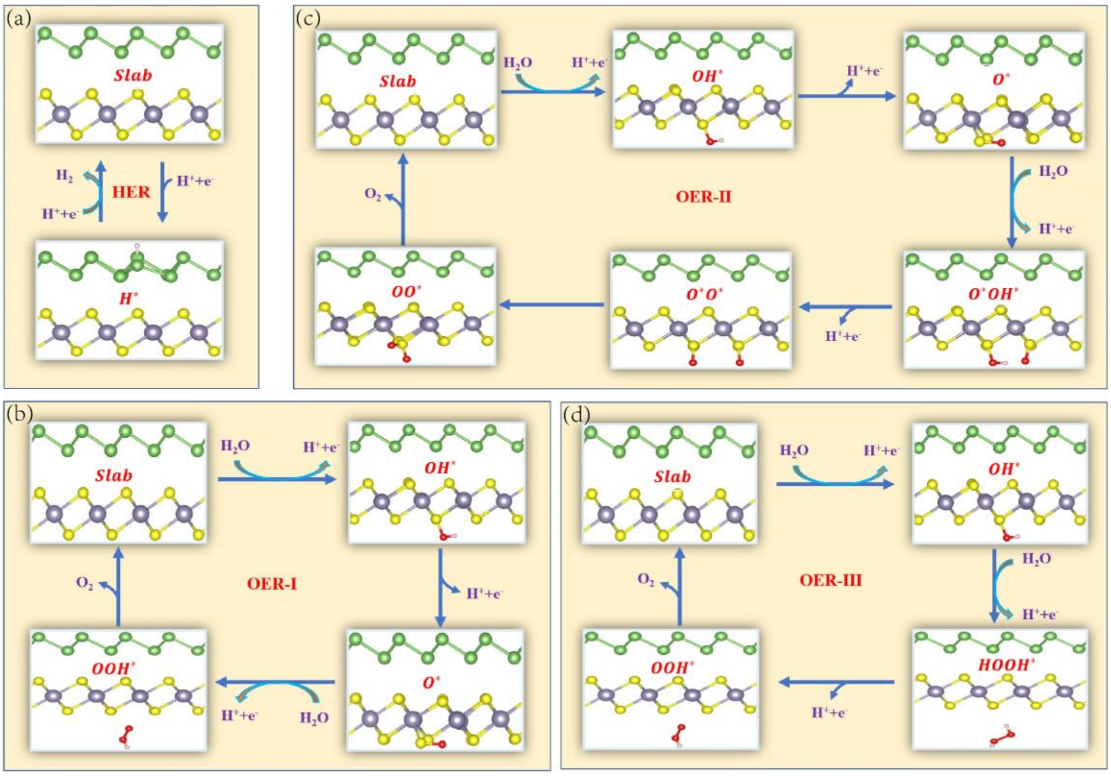

Figure S4 The intermediate states and adsorption sites of (a) HER, (b) OER-I, (c) OER-II and (d) OER-III in the SnS_2/β-As heterostructure.

Spectral absorption

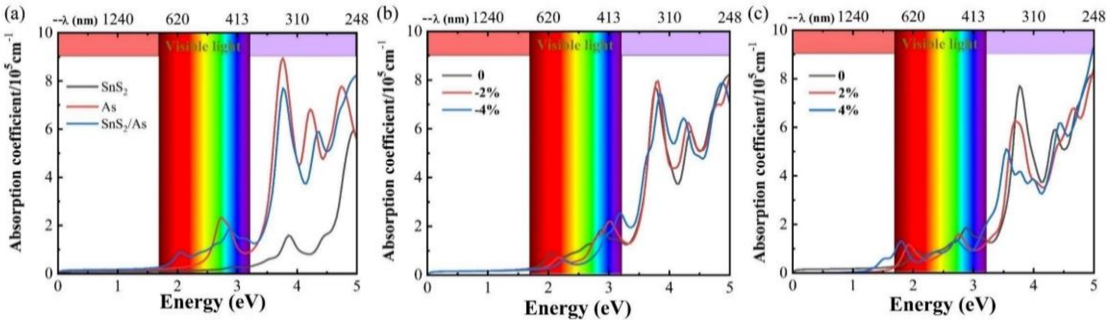

Figure S5 (a) spectral absorption of SnS_2, β-As and SnS_2/β-As without strain; spectra absorption of (b) negative and (c) positive strains of the SnS_2/β-As heterostructure.

Atomic coordinates

Table S1 Atomic fraction coordinates in SnS_2 and β-As nanosheets unit cells, and atomic fraction coordinates in SnS_2/β-As heterostructure with AB-stacking.

	a	**b**	**c**
β-As - unit cell	0.367063	0.597467	0.25061
	0.700397	0.264133	0.19476
	0.000000	0.000000	0.500000
SnS_2 - unit cell	0.333332	0.666668	0.564624
	0.666668	0.333332	0.435376
	-0.00062	0.001908	0.415266
	0.499381	0.001908	0.415266
	-0.00062	0.501908	0.415266
	0.499381	0.501908	0.415266
SnS_2/β-As heterostructure （2×2）	0.165987	0.335632	0.468391
	0.332711	0.168522	0.362254
	0.665987	0.335632	0.468391
	0.832711	0.168522	0.362254
	0.165987	0.835632	0.468391
	0.332711	0.668522	0.362254

	a	b	c
	0.665987	0.835632	0.468391
	0.832711	0.668522	0.362254
	0.164491	0.345702	0.625348
	0.331159	0.179036	0.576211
	0.664491	0.345702	0.625348
	0.831159	0.179036	0.576211
	0.164491	0.845702	0.625348
	0.331159	0.679036	0.576211
	0.664491	0.845702	0.625348
	0.831159	0.679036	0.576211

Table S2 The structural parameters, including lattice constant a; the bond lengths of Sn-S (d_1), As-As (d_2); the distance between the layers (d); the bond angles of Sn-S-Sn (θ_1), S-Sn-S (θ_2), As-As-As (θ_3); the bandgap E_g (PBE/HSE06) of SnS_2/β-As heterostructure with AB-stacking, AC-stacking, and AD-stacking; the binding energy E.

Structure	a(Å)	d_1(Å)	d_2(Å)	d(Å)	θ_1	θ_2	θ_3	E_g(eV)	E(eV)
AB	7.36	2.59	2.53	3.02	90.44°	89.54°	93.31°	0.31/0.89	-0.76
AC	7.36	2.59	2.53	3.73	90.37°	89.54°	93.25°	0.37/-	-0.46
AD	7.36	2.59	2.53	3.15	90.47°	89.52°	93.36°	0.18/-	-0.70

References

(1) Wang, G.; Li, Z.; Wu, W.; Guo, H.; Chen, C.; Yuan, H.; Yang, S. A. A Two-Dimensional h-BN/C_2N Heterostructure as a Promising Metal-Free Photocatalyst for Overall Water-Splitting. *Phys. Chem. Chem. Phys.* **2020**, *22*, 24446-24454.
(2) Ren, K.; Tang, W.; Sun, M.; Cai, Y.; Cheng, Y.; Zhang, G. A Direct Z-Scheme PtS_2/Arsenene Van der Waals Heterostructure with High Photocatalytic Water Splitting Efficiency. *Nanoscale* **2020**, *12*, 17281-17289.
(3) Zhou, Z.; Yuan, S.; Wang, J. Theoretical Progress on Direct Z-Scheme Photocatalysis of Two-Dimensional Heterostructures. *Front Phys.* **2021**, *16*, 43203.
(4) Yin, S.; Zhao, X.; Jiang, E.; Yan, Y.; Zhou, P.; Huo, P. Boosting Water Decomposition by Sulfur Vacancies for Efficient CO_2 Photoreduction. *Energy Environ. Sci.* **2022**, *15*, 1556-1562.
(5) Cheng, H.; Cheng, J.; Wang, L.; Xu, H. Reaction Pathways toward Sustainable Photosynthesis of Hydrogen Peroxide by Polymer Photocatalysts. *Chem. Mater.* **2022**, *34*, 4259-4273.
(6) Wu, Y. B.; He, C.; Han, F. S.; Zhang, W. X. Construction of an Arsenene/g-C_3N_4 Hybrid Heterostructure Towards Enhancing Photocatalytic Activity of Overall Water Splitting: A First-Principles Study. *J Solid State Chem* **2021**, *299*, 122138.
(7) Lin, S.; Ye, X.; Gao, X.; Huang, J. Mechanistic Insight into the Water Photooxidation on Pure and Sulfur-Doped g-C_3N_4 Photocatalysts from DFT Calculations with Dispersion Corrections. *J Mol Catal A Chem.* **2015**, *406*, 137-144.
(8) Wan, Y.; Wang, L.; Xu, H.; Wu, X.; Yang, J. A Simple Molecular Design Strategy for Two-Dimensional Covalent Organic Framework Capable of Visible-Light-Driven Water Splitting. *J. Am. Chem. Soc.* **2020**, *142*, 4508-4516.
(9) He, C.; Han, F.; Zhang, W. The InSe/g-CN Van Der Waals Hybrid Heterojunction as a Photocatalyst for Water Splitting Driven by Visible Light. *Chin Chem Lett.* **2022**, *33*, 404-409.
(10) Li, J.; Huang, Z.; Ke, W.; Yu, J.; Ren, K.; Dong, Z. High Solar-to-Hydrogen Efficiency in Arsenene/GaX (X = S, Se) Van Der Waals Heterostructure for Photocatalytic Water Splitting. *J. Alloys Compd.* **2021**, *866*, 158774.
(11) Cao, M.; Ni, L.; Wang, Z.; Liu, J.; Tian, Y.; Zhang, Y.; Wei, X.; Guo, T.; Fan, J.; Duan, L. DFT Investigation on Direct Z-Scheme Photocatalyst for Overall Water Splitting: $MoTe_2$/BAs Van Der Waals Heterostructure. *Appl. Surf. Sci.* **2021**, *551*, 149364.

(12) Li, H.; Zhang, H.; Xiong, Y.; Ye, L.; Li, W. Van Der Waals Heterostructures Based on SiC-BS: A Promoted Photocatalytic Properties for Water Splitting. *Physics Letters A* **2021**, *410*, 127514.
(13) Liu, J.; Chen, S.; Liu, Q.; Zhu, Y.; Lu, Y. Density Functional Theory Study on Electronic and Photocatalytic Properties of Orthorhombic $AgInS_2$. *Comput. Mater. Sci.* **2014**, *91*, 159-164.
(14) Yang, W.; Wen, Y.; Zeng, D.; Wang, Q.; Chen, R.; Wang, W.; Shan, B. Interfacial Charge Transfer and Enhanced Photocatalytic Performance for the Heterojunction WO_3/BiOCl: First-Principles Study. *J. Mater. Chem. A* **2014**, *2*, 20770-20775.
(15) Liu, X.; Jiang, B.; Liu, Y.; Liu, L.; Xia, T.; Zhang, X.; Ye, C.; Yu, Y.; Wang, B. Two-Dimensional As/Bluep Van Der Waals Hetero-Structure as a Promising Photocatalyst for Water Splitting: A DFT Study. *Coatings* **2020**, *10*, 1160.